Intercellular calcium waves in glial cells with bistable dynamics

2011 Phys. Biol. 8 026009

(http://iopscience.iop.org/1478-3975/8/2/026009)

Phys. Biol. **8** (2011) 026009 (10pp) doi:10.1088/1478-3975/8/2/026009

Intercellular calcium waves in glial cells with bistable dynamics

Fang Wei and Jianwei Shuai

Department of Physics and Institute of Theoretical Physics and Astrophysics, Xiamen University, Xiamen 361005, People's Republic of China

E-mail: jianweishuai@xmu.edu.cn

Received 13 December 2010
Accepted for publication 16 December 2010
Published 4 March 2011
Online at stacks.iop.org/PhysBio/8/026009

Abstract

A two-dimensional model is proposed for intercellular calcium (Ca^{2+}) waves with Ca^{2+}-induced IP_3 regeneration and the diffusion of IP_3 through gap junctions. Many experimental observations in glial cells, i.e. responding to local mechanical stimulation, glutamate application, mechanical stimulation followed by ACh application, and glutamate followed by mechanical stimulation, are reproduced and classified by the model. We show that a glial cell model with bistable dynamics, i.e. a Ca^{2+} oscillation state coexisting with a fixed point, can cause a prolonged plateau of Ca^{2+} signals in the cells nearby the stimulated cell when the cell network responds to the local mechanical stimulation.

1. Introduction

Calcium waves are as prevalent in astrocytes as action potentials in neurons. The long-range intercellular calcium (Ca^{2+}) signals provide a mechanism for the integration and transmission of information between cells [1–5]. In glial cells, experiments confirmed a direct role of Ca^{2+} signals in modulating the neuronal excitability and synaptic transmission with the release of the transmitter glutamate [6, 7], although the detailed dynamics are still under investigation [8].

Intercellular Ca^{2+} wave (ICW) can be induced in responding to bath application of glutamate or ATP in glial cells [1, 2]. Mechanical or electrical stimulation can also generate the ICWs [2, 3, 9–11]. Intracellularly, Ca^{2+} signals in glial cell result from the release of Ca^{2+} from intracellular stores, e.g. endoplasmic reticulum (ER), through the inositol-1,4,5-trisphospate receptor (IP_3R) channel. IP_3Rs can be open upon the bindings of Ca^{2+} ion and the second messenger inositol-1,4,5-trisphospate (IP_3). Two different types of intracellular Ca^{2+} waves were observed in the experiment responding to the local mechanical stimulation: an oscillatory Ca^{2+} response [1–3, 11] or a single sustained Ca^{2+} transient [4, 5, 9, 10].

A basic question concerning the intercellular Ca^{2+} signals is the mechanism how the signal can spread to neighboring glial cells to produce ICWs. Compelling data show that the permeability of intracellular IP_3 messenger or Ca^{2+} ions through gap junctions and the spreading of extracellular ATP messenger are important mechanisms for ICWs [1–7, 12]. However, the extent to which Ca^{2+} waves depend on intracellular or extracellular messengers appears to be species-specific and under certain physiological conditions [9, 10, 13]. Many studies suggest that in rat glial cells the mechanism to propagate Ca^{2+} waves, induced by mechanical stimulus or a focal application of neurotransmitters, appears to rely mainly on the intercellular diffusion of IP_3 through gap junctions [2, 5, 11].

Understanding of intercellular Ca^{2+} processes can be greatly facilitated by mathematical modeling [14–24]. Different ICW models have been proposed, to simulate either the oscillatory Ca^{2+} response [14–19] or the sustained Ca^{2+} transient [20–24]. Different coupling mechanisms among cells have been investigated, including the IP_3 gap-junction diffusion [16, 18–20], the Ca^{2+} gap-junction diffusion [15, 17, 21, 22], both the IP_3 and Ca^{2+} diffusions through gap junction [23], or the extracellular diffusion of messengers ATP and UTP together with the IP_3 gap-junction diffusion [24]. A nonlinear gap junction for IP_3 diffusion has recently been suggested also for long-distance regenerative ICWs [14].

A widely simulated experiment is the ICWs induced by local mechanical stimulation. The mechanical stimulation induces a high IP_3 concentration in the stimulated cell. For those models with IP_3 diffusion through gap junctions [16, 18–20], the IP_3 messenger can directly propagate into the

nearby cells, setting up a spatial gradient of IP_3 across the cell network and causing different patterns of Ca^{2+} signals in different cells. It has been suggested that the Ca^{2+}-induced IP_3 regeneration is not a necessary term [18–20]. Later, Hofer *et al* showed that a model with IP_3 regeneration and gap-junction diffusion is indeed compatible with the limited spatial range of ICWs observed in the experiments and can account for many of the observed features of wave propagation, such as the realistic wave ranges and the sensitivity of the wave range to the stimulus [23]. With a two-cell coupled model, Ullah *et al* indicated that Ca^{2+}-induced IP_3 regeneration is a necessary factor in order to observe the anti-phase synchronization observed in experiment [25].

In the paper, we study the ICWs with oscillatory Ca^{2+} signals. A prominent feature observed in experiment is that the glial cells show a very prolonged oscillating Ca^{2+} signals (more than 160 s) responding to a local mechanical stimulation [11, 19]. Although the oscillatory ICW models in [14–19] can reproduce many experimental observations, the ICW responding durations predicted by these models are typically less than 100 s [18, 19]. Besides the experiment with local mechanical stimulation [2, 3, 9, 11], some other experimental observations in glial cells, i.e. glutamate application [1, 2], mechanical stimulation followed by ACh application [11, 19] and glutamate followed by mechanical stimulation [2], are seldom discussed with mathematical models systematically [15–24].

An ICW model is proposed here with the IP_3 diffusion through gap junctions and a small term of Ca^{2+}-induced IP_3 regeneration. Different from most of the ICW models [14–25], our model has bistability behavior (i.e. an oscillating state coexisting with a fixed point) in a large parameter range. Many behaviors of the intracellular Ca^{2+} oscillations are related to the bistable states. We show that, with such bistable states and the IP_3 regeneration dynamics, the model can produce a very prolonged Ca^{2+} signal responding to a mechanical stimulation, as observed in experiment [11]. Furthermore, we use the model to systematically discuss various experimental results of glia cells, responding not only to local mechanical stimulation [2, 3, 9, 11] but also to glutamate application [1, 2], mechanical stimulation followed by ACh application [11, 19] and glutamate followed by mechanical stimulation [2].

2. Theoretical model

2.1. The Ca^{2+} dynamics

In the model, each cell is spatially extended on a two-dimensional plane. A schematic diagram for Ca^{2+} and IP_3 dynamics in the model is given in figure 1(*A*). The Ca^{2+} elevation resulting from the release of Ca^{2+} from ER is controlled by three calcium fluxes: the channel flux J_C from the ER to the intracellular space through the IP_3R channels, the pump flux J_P from the intracellular space into the ER, and the leakage flux J_L from the ER to the intracellular space. All these three fluxes are assumed to be distributed on the ER membrane homogeneously. We ignore the cluster distribution

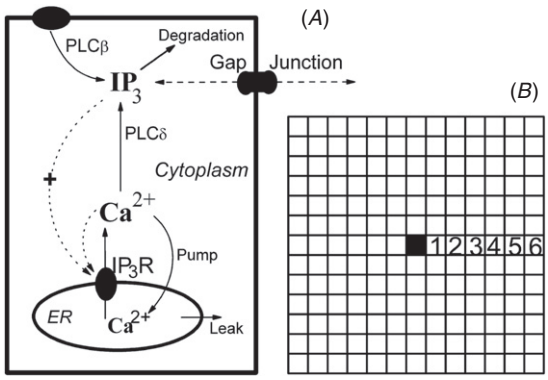

Figure 1. Scheme of the Ca^{2+} and IP_3 dynamics in the cell model (*A*) and network structure of 13×13 cells (*B*). Nearby cells are coupled by IP_3 permeability through the gap junction.

of IP_3Rs on the ER membrane [26, 27]. The extrusion and entry of cytosol Ca^{2+} across the plasma membrane are ignored in the model. Considering the effective diffusion approach for free Ca^{2+} with its buffers, the intracellular diffusion of Ca^{2+} is written as

$$\frac{\partial C(x,y)}{\partial t} = D_C \nabla^2 C(x,y) + J_C - J_P + J_L \tag{1}$$

where C is the concentration of Ca^{2+} in the cytoplasm and D_C is the effective diffusion constant.

Various models have been proposed for IP_3R channels [28–32]. In our model we use a simple model proposed by Li and Rinzel [29]. The Li–Rinzel model assumes that three equivalent and independent subunits are involved in the conduction of an IP_3R. Each subunit has one IP_3 binding site (m gate) and two Ca^{2+} binding sites, one for activation (n gate) and the other for inhibition (h gate). The m and n gates are substituted by their steady states, m_∞ and n_∞, due to their fast time scales. So the channel flux is given as

$$J_C = v_C m_\infty^3 n_\infty^3 h^3 (C - C_E), \tag{2}$$

with

$$\begin{aligned} m_\infty &= \frac{I}{I + d_I}, \\ n_\infty &= \frac{C}{C + d_C}, \end{aligned} \tag{3}$$

where I is the concentration of IP_3 in the cytoplasm and C_E the Ca^{2+} concentration in the ER pool. Due to its slow time scale, the h gate is considered as a variable in the model [29]:

$$\frac{\mathrm{d}h(x,y)}{\mathrm{d}t} = \alpha_h(1-h) - \beta_h h, \tag{4}$$

with the opening rate α_h and closing rate β_h given as

$$\begin{aligned} \alpha_h &= a_1 \frac{I + d_1}{I + d_2}, \\ \beta_h &= a_2 C. \end{aligned} \tag{5}$$

The other two Ca^{2+} fluxes are read as [28, 29]

$$J_P = v_P \frac{C^2}{k_P^2 + C^2}, \tag{6}$$

$$J_L = v_L (C - C_E). \tag{7}$$

Here, v_C, v_P and v_L denote the rates of channel flux, pump flux and leakage flux of Ca^{2+}.

2.2. The IP_3 dynamics

In the model, we consider two distinct production terms for IP_3 (figure 1(*A*)): one is a constant generation source J_β for IP_3 as a consequence of the steady activity of phosphoinositide-specific phospholipase C (PLCβ) [23]. The other one J_δ is the production of IP_3 by PLCδ activity, giving a positive feedback between Ca^{2+} and IP_3 [23, 25, 33, 34]. Considering the intracellular diffusion of IP_3 in the cytoplasm and an IP_3 degradation dynamics J_D [19], we have

$$\frac{\partial I(x,y)}{\partial t} = D_I \nabla^2 I(x,y) + J_\beta - J_D + J_\delta + J_{\text{stim}}, \tag{8}$$

with

$$J_D = v_D \frac{I}{K_D + I}, \tag{9}$$

$$J_\delta = v_\delta \frac{C^2}{K_\delta^2 + C^2}, \tag{10}$$

where D_I is the diffusion coefficient for cytoplasmic IP_3, v_D the IP_3 degradation rate, and v_δ the Ca^{2+}-induced IP_3 generation rate.

In the model we use J_{stim} to simulate various stimulations applied to the cells. In experiment, in order to induce a large IP_3 concentration locally one can stimulate a single glial cell mechanically by briefly deforming the cell surface [2, 11]. Correspondingly, we consider a term J_{stim}^M for the stimulated cell to represent the large IP_3 generation rate caused by the local stimulation. Following Sneyd *et al* [19], we typically set $J_{\text{stim}} = 1.0\ \mu\text{M}\,\text{s}^{-1}$ in equation (8) to the central stimulated cell for 15 s to simulate a local mechanical stimulation.

The bath application of glutamate or ACh in glial cells is also used in the experiments to cause the production of IP_3 in the glial cells [1, 3]. In the model, the glutamate and ACh bath applications are simply represented by stimulation terms J_{stim}^G or J_{stim}^A, respectively, applied in all the cells. Although glutamate and ACh applications will trigger different signal pathways to generate IP_3 messengers and so there may be different dose-responding functions for IP_3 generation rate on the glutamate and ACh [25, 33, 34], but the main concern in the model is that a certain IP_3 generation rate will be determined upon the application of a certain dose of glutamate or ACh bath. Thus, the IP_3 responses to bath application of glutamate and ACh are both simply modeled by the generating rate J_{stim} in the model.

2.3. Cell network coupled with gap junction

A two-dimensional network of 13×13 glial cells is considered (figure 1(*B*)). In the cell network, neighboring cells are coupled by gap junctions that are assumed to permeate IP_3 only. Following the previous models [18–20, 23], we simply assume that the gap junctions are homogeneously distributed through the whole boundary of cell and so at each cell coupling boundary the intercellular IP_3 flux conditions read as [18]

$$D_I \nabla I \cdot \mathbf{n} = P_I (I_+ - I_-), \tag{11}$$

where P_I is the gap junctional permeability for IP_3, I_+ and I_- denote the IP_3 concentrations on either side of the boundary, and $\mathbf{n}$ is the unit normal vector to the boundary.

Table 1. Parameters of the model.

Parameter	Value	Parameter	Value
Diffusion	Parameters	Ca^{2+} model	Parameters
D_C	20.0 $\mu\text{m}^2\,\text{s}^{-1}$	C_E	4.0 μM
D_I	280.0 $\mu\text{m}^2\,\text{s}^{-1}$	v_C	2.2 s^{-1}
P_I	0.5 $\mu\text{m}\,\text{s}^{-1}$	v_L	0.002 s^{-1}
		v_P	0.4 $\mu\text{M}\,\text{s}^{-1}$
IP_3 model	parameters	k_P	0.025 μM
v_D	0.05 $\mu\text{M}\,\text{s}^{-1}$	d_I	0.12 μM
K_D	1.0 μM	d_C	0.02 μM
v_δ	0.004 $\mu\text{M}\,\text{s}^{-1}$	d_1	0.13 μM
K_δ	0.1 μM	d_2	0.9 μM
J_β	0.006 $\mu\text{M}\,\text{s}^{-1}$	a_1	0.4 s^{-1}
		a_2	0.4 $\mu\text{M}^{-1}\,\text{s}^{-1}$

2.4. Parameter selection and numerical method

The parameter values of the ICW model are listed in table 1. The effective Ca^{2+} and IP_3 diffusion constants D_C and D_I are the typical values measured by Allbritton *et al* [35]. The parameters related to the Ca^{2+} dynamics in equations (1)–(7) are mainly based on the Li–Rinzel model [29] and adjusted in order to give a Ca^{2+} oscillation as observed in the experiment. The sensitive parameters affecting the ICWs are the parameters related to the IP_3 dynamics in equations (8)–(11). Here the IP_3 degradation rate v_D is taken from the experimental fitting with N1E-115 neuroblastoma cells [36]. K_D is obtained from the simulation model [19]. The generation rate $J_\beta = 0.006\ \mu$M is applied, resulting in the IP_3 concentration 0.137 μM and the Ca^{2+} concentration 0.007 μM at steady state.

As indicated by Sneyd *et al* [18], IP_3 permeability P_I is quite an important parameter for ICWs. The ICW model simulations suggest that a large value of 1–5 $\mu\text{m}\,\text{s}^{-1}$ is expected [18–20, 23]. However, it was estimated that the permeability of IP_3 is about 0.1–0.4 $\mu\text{m}\,\text{s}^{-1}$ in glial cells, airway epithelium cells, earthworm giant axon septate membrane and intercalated disks of myocardium [18]. In our model, a value of $P_I = 0.5\ \mu\text{m}\,\text{s}^{-1}$ is typically used.

We solve the model equations numerically by using the forward Euler algorithm with C language for programming. The cell network consists of 13×13 cells in the simulation. Each cell has a size of 24 μm $\times$ 24 μm, represented by 12×12 regular square grid points with spatial discretization length of $\text{d}x = 2\ \mu$m. The time increment is $\text{d}t = 2$ ms. The IP_3 messengers, but not Ca^{2+} ions, are permeable between the cells. The intercellular IP_3 permeability are numerically solved by a first-order approximation of the fluxes across the membrane proposed by [20, 22]. Actually we use the numerical methods previously described in the appendix in [22]. The no-flux boundary conditions around the edge of cell network are applied. Simulation with more grid points in each cell or with more number of cells in the network shows no significant differences from the results given here.

Initially, every cell is set at the steady state with $C = 0.007\mu$M and $I = 0.137\ \mu$M corresponding to $J_\beta = 0.006\ \mu\text{M}\,\text{s}^{-1}$ without any external stimulation.

3. Results

3.1. The point model

If we consider large intracellular diffusions for IP_3 and Ca^{2+} and preclude the intercellular permeability of IP_3, a point model is obtained for the intracellular Ca^{2+} signals. Such a point model consists of equations (1)–(10) with $D_C = 0$ and $D_I = 0$. Using the software XPPAUT, the bifurcation diagrams of Ca^{2+} and IP_3 concentrations as a function of J_{stim} are plotted in figures 2(*A*) and (*B*), respectively. The stable fixed points (SF) are plotted with the solid blue lines and the maxima and the minima of stable periodic oscillations (SP) are plotted with the solid red lines.

From figure 2, four typical regimes with different Ca^{2+} dynamics can be distinguished: regime I with a fixed point at $J_{stim} < 0.0003\ \mu M\,s^{-1}$, regime II with a periodic oscillation at $0.0003 < J_{stim} < 0.0006\ \mu M\,s^{-1}$, regime III with bistable states of a periodic oscillation and a fixed point at $0.0006 < J_{stim} < 0.005\ \mu M\,s^{-1}$, and regime IV with a fixed point at $J_{stim} > 0.005\ \mu M\,s^{-1}$. The period of the oscillating state decreases from 41 to 12.5 s with the increase of J_{stim} in regimes II and III.

In this point model, the interactions of Ca^{2+} and IP_3 are mutual due to an IP_3-induced Ca^{2+} release (J_C in equation (1)) and a Ca^{2+}-induced IP_3 generation (J_δ in equation (8)). However, because of the small term of Ca^{2+}-induced IP_3 generation J_δ, the IP_3 messenger shows a very small oscillating amplitude in the oscillatory state. As a result, as plotted in figure 2(*B*), the four regimes of J_{stim} also simply correspond to the four regimes of the IP_3 concentration.

Actually the Ca^{2+} dynamics can be roughly understood with the point model at $J_\delta = 0$ in equation (8), i.e. ignoring Ca^{2+}-induced IP_3 generation. With $J_\delta = 0$, the IP_3 concentration increases with the increase of J_{stim}. Then the Ca^{2+} dynamics are simply modulated by the IP_3 concentration, and the model becomes the Li–Rinzel model described by equations (1)–(7). The bifurcation diagram of the Ca^{2+} concentration as a function of IP_3 for the Li–Rinzel model is plotted in figure 2(*C*). Figure 2(*C*) clearly shows that the four different Ca^{2+} dynamics are related to four regimes of the IP_3 concentration, i.e. regime I at $I < 0.14\ \mu M$, regime II at $0.14 < I < 0.25\ \mu M$, regime III at $0.25 < I < 0.38\ \mu M$, and regime IV at $I > 0.38\ \mu M$, which are almost the same as the four regimes of IP_3 plotted in figure 2(*B*).

With the equilibrium bifurcation diagram, the dynamical Ca^{2+} behaviors responding to the slow change of the IP_3 concentration (or J_{stim}) can be understood. For example, starting at $I = 0$, the slow increase of I causes a small increase of Ca^{2+} with fixed point dynamics. Once $I > 0.14\ \mu M$ in regimes II and III, the Ca^{2+} signal becomes an oscillatory dynamics. When the increasing I goes into regime IV ($I > 0.38\ \mu M$), the Ca^{2+} dynamics changes back to a fixed point. However, if starting at regime IV with $I > 0.38\ \mu M$, the decreasing I will generate a fixed point for Ca^{2+} signal until $I = 0.25\ \mu M$. Then an oscillatory Ca^{2+} signal will be born only when I is in regime II. Such an oscillation will die and a fixed point of Ca^{2+} will be generated when $I < 0.14\ \mu M$ in regime I.

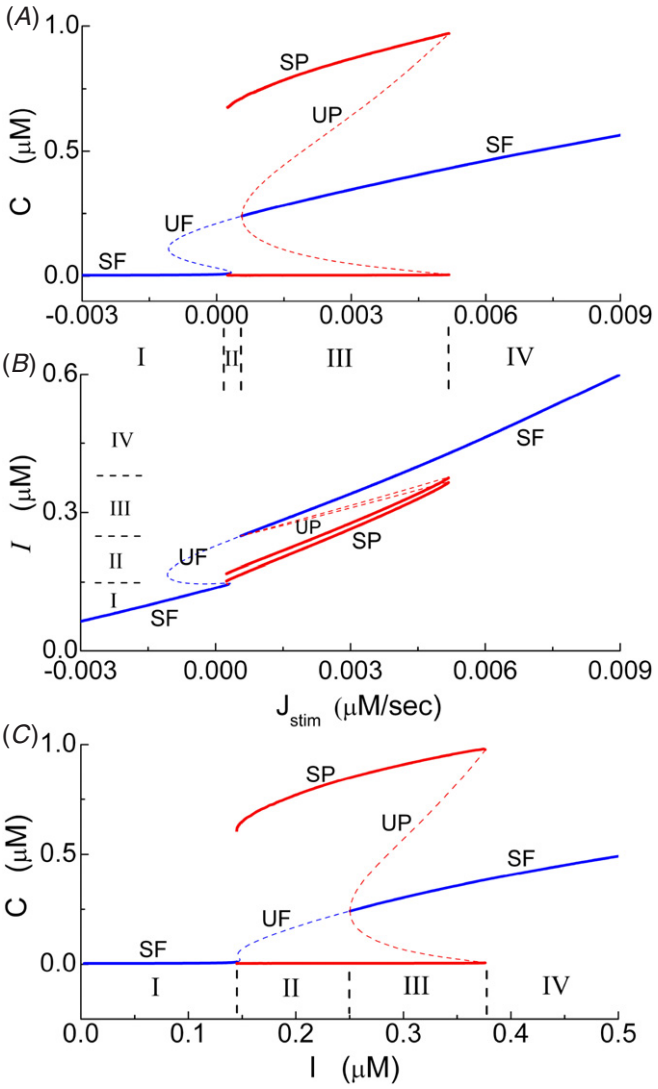

Figure 2. The bifurcation diagram of the Ca^{2+} concentration (*A*) and the IP_3 concentration (*B*) versus J_{stim} for the point model given by equations (1)–(10) with $D_C = 0$ and $D_I = 0$, and (*C*) the bifurcation diagram of the Ca^{2+} concentration versus the IP_3 concentration for the Li–Rinzel model given by equations (1)–(7) with $D_C = 0$. The solid blue lines represent the stable fixed point (SF); the solid red lines represent the maximum and the minimum of stable periodic oscillation (SP); the dashed blue lines represent the unstable fixed point (UF), and the dashed red lines represent the maximum and the minimum of unstable periodic oscillation (UP).

In the following sections, we will show that many behaviors of the intracellular Ca^{2+} oscillations in each spatially extended cell are related to the bistable states discussed in the point model.

3.2. Local mechanical stimulation

A widely studied ICW is induced by the mechanical stimulation locally on a single cell in the primary rat glial culture [2, 3, 9, 11]. Mechanical stimulation of a glial cell causes a local elevation of IP_3 that subsequently spreads to its neighbors, resulting in an ICW. Different responding Ca^{2+} patterns are observed in different cells in the experiment (see figure 4 in [11]). For the cells which are close to the

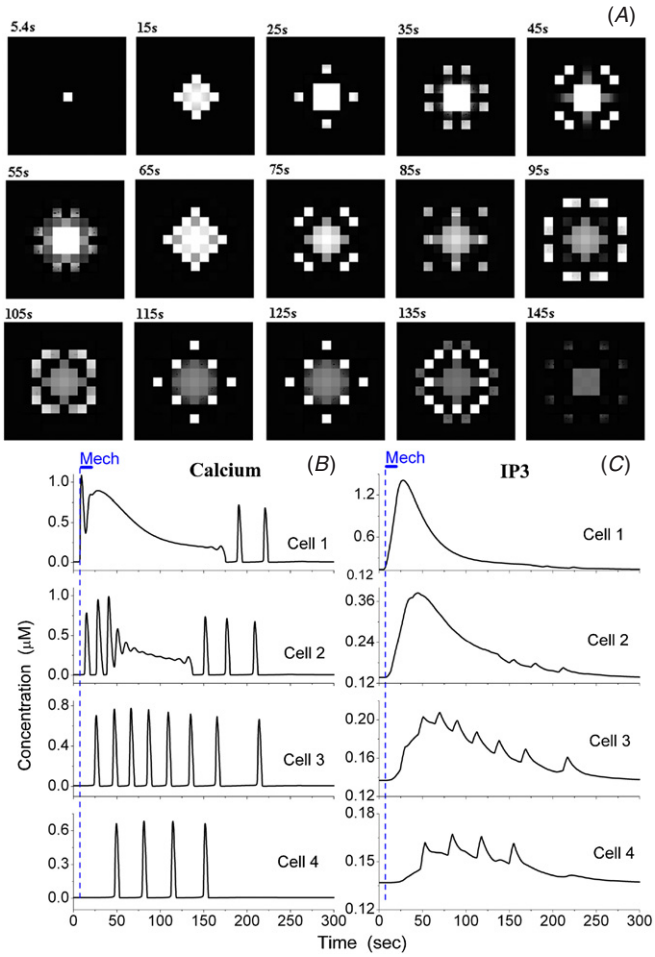

Figure 3. The Ca^{2+} and IP_3 waves responding to the local mechanical stimulation. (*A*) The snapshots of intercellular Ca^{2+} waves in the cell network; (*B*) the Ca^{2+} signals in cells 1, 2, 3, and 4, respectively, and (*C*) the IP_3 signals in cells 1, 2, 3, and 4, respectively. In all the gray patterns, the white dots represent $C = 0.5$ μM and the black dots $C = 0$ μM. In all the trace figures, the trajectories of Ca^{2+} and IP_3 concentrations are obtained from the central grid of the corresponding cells. The dashed blue line represents the local mechanical stimulation with 15 s duration.

stimulated cell, the spike-type signal occurs, characterized by the quick onset of a rapid burst of spikes in Ca^{2+}, following a prolonged high Ca^{2+} plateau. For the cells which are next to the spike-type cells, the responding patterns are typically the continuous-type or brief-type oscillations. Further away from the stimulated cell, very little rise in Ca^{2+} can be observed in response to the stimulation [11]. Typically, less than 100 cells show Ca^{2+} responding waves [5].

In our model, the stimulated cell is located at the central of the 13 × 13 cell network, i.e. the blacked cell shown in figure 1(*B*). At first all the glial cells are in the steady state. Starting from $t = 5$ s we set $J_{\text{stim}}^{M} = 1.0$ μM s^{-1} for 15 s in equation (8) to the central cell to simulate a mechanical stimulation. The simulation results with the parameters listed in table 1 are given in figure 3.

Figure 3(*A*) shows the snapshots of intercellular Ca^{2+} waves with time interval of 10 s. Because of the symmetry of the model assumptions, symmetric ICWs are observed in figure 3(*A*). Upon local mechanical stimulation, the responding Ca^{2+} waves only travel 4 cells in any direction in this example, involving totally 68 responding cells. There are 80% cells, i.e. 56 cells out of 68 cells, showing oscillatory response. So oscillating wave is the most prominent group, as observed in experiment [11]. The spreading speeds of the intracellular Ca^{2+} waves are varying between 25 and 40 μm s^{-1} at different cells and depending on the IP_3 concentration. The latencies of Ca^{2+} signal spreading from one cell to the nearby cell increase from 4 to 40 s with the increase of the distance from the stimulated cell.

Figures 3(*B*) and (*C*) plot the trajectories of Ca^{2+} and IP_3 at the central grid in cells 1, 2, 3 and 4 (see figure 1(*B*) for cell positions), respectively. In all the following figures, the trajectories of Ca^{2+} or IP_3 concentrations are obtained from the central grid in the cells.

As shown in figures 3(*B*) and (*C*), different types of Ca^{2+} waves are observed in different cells. For cell 1, soon after the application of mechanical stimulation at the central cell, the large IP_3 influx permeating from the central cell builds up a high IP_3 concentration. The first Ca^{2+} spike shown in cell 1 in figure 3(*B*) corresponds to the transient oscillation due to the fast increase of IP_3 passing through regimes II and III (regimes marked in figure 2). The increasing IP_3 concentration soon goes into regime IV with $I > 0.38$ μM and the cell shows a fixed point dynamics with a large Ca^{2+} concentration. After the stimulation, because of the less and less IP_3 influx from the stimulated cell and the more and more IP_3 efflux to the other nearby cells (such as cell 2), as well as the IP_3 degradation, the IP_3 concentration increases first and then decreases gradually. As long as the IP_3 concentration is in regimes IV and III ($I > 0.25$ μM), the cell typically shows a fixed point dynamics, giving a long but decaying Ca^{2+} plateau. Then after a short duration of transient Ca^{2+} oscillation with IP_3 in regime II, cell 1 finally settles down at the steady state with the steady IP_3.

In the experiment, a Ca^{2+} plateau is observed lasting more than 160 s for the cells close to the stimulated cell [11]. In the model the Ca^{2+} plateau in cell 1 prolongs to 175 s and the responding signal is as long as 225 s (cell 1 in figure 3(*B*)). A long Ca^{2+} plateau obtained in the model is because, even when the decreasing IP_3 falls into oscillating regime III, the cell model still keeps the fixed point dynamics. For the simulation, one can apply a larger J_{stim} with a longer duration easily in order to induce a longer Ca^{2+} plateau in cell 1. But such a stronger stimulus will also easily involve more responding cells in the network than those observed in experiment [5].

The farther cells, e.g. cells 3 and 4, show a continuous Ca^{2+} oscillation behavior. For these cells the permeating IP_3 influx, acting as the term J_{stim}, typically drives the cell into the oscillating regime II or then III with $0.14 < I < 0.38$ μM, causing an oscillatory dynamics only. From figure 3(*B*), one can also see that the subsequent Ca^{2+} oscillations induced in cells 3 and 4 occur at different time with different instant periods. Even for the same cell, the instant oscillating periods become longer and longer with time due to the decaying IP_3. The instant periods of intracellular Ca^{2+} waves are varying from 13 to 50 s. Similar results are also observed in experiment [11].

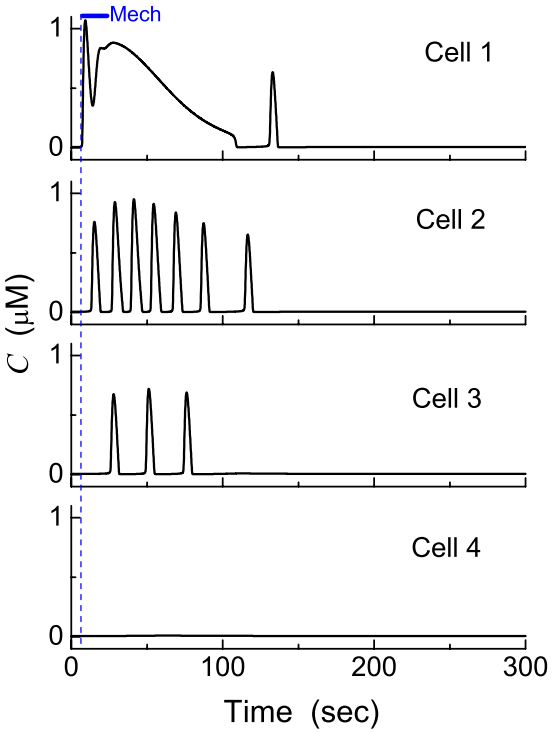

Figure 4. Effect of calcium-induced IP_3 generation on the ICWs. The figure shows the Ca^{2+} signals of cells 1, 2, 3, and 4 at $v_\delta = 0.0\ \mu M\,s^{-1}$, respectively. The dashed blue line represents the local mechanical stimulation with 15 s duration.

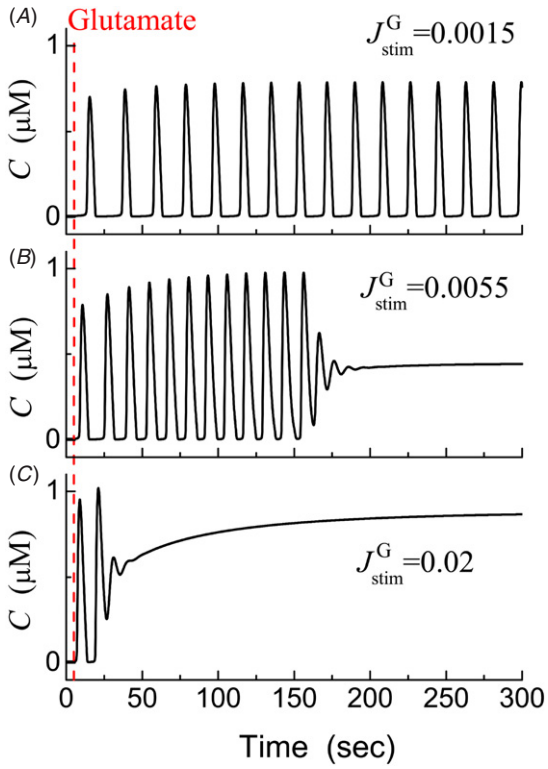

Figure 5. ICWs responding to the application of glutamate bath. (*A*) $J^G_{stim} = 0.0015\ \mu M\,s^{-1}$ in the oscillatory dynamics regime; (*B*) $J^G_{stim} = 0.0055\ \mu M\,s^{-1}$ and (*C*) $J^G_{stim} = 0.02\ \mu M\,s^{-1}$ in the fixed point regime. The Ca^{2+} trajectories are obtained at the central grid in the center cell of the network. The dashed line represents the application of the glutamate bath.

For cell 2, which is located between cells 1 and 3, it shows a mixed behavior of the plateau-type and oscillation-type. At first, the IP_3 concentration in cell 2 increases slowly (figure 3(*C*)). Similar to cell 3, the permeating IP_3 influx first drives the IP_3 into the regime II and then into III, generating an oscillatory Ca^{2+} signal. Then, at time 40 s, the cell model is driven into regime IV with a high IP_3 concentration with $I > 0.38\ \mu M$, resulting soon in a Ca^{2+} plateau due to the fixed point dynamics. Later, the IP_3 starts to decay. Similar to cell 1, cell 2 keeps with the fixed-point dynamics as long as the IP_3 concentration is in regimes IV and III. Once the decreasing IP_3 goes into regime II with $0.14 < I < 0.25\ \mu M$, an oscillatory Ca^{2+} signal will be born again. As a result, cell 2 shows a damped Ca^{2+} oscillation followed by a prolonged plateau and then another duration of slow oscillation (cell 2 in figure 3(*B*)).

The three types of Ca^{2+} patterns (cell 1, cell 2, and cells 3 and 4) represent the three commonly observed patterns in experiment, i.e. the spiking, brief and continuous waves (see figure 4 in [11]). There is not only Ca^{2+} wave initiated in cells 5 and 6 because the change of IP_3 concentration is very small due to the weak permeation of IP_3 through the gap junction.

Now we discuss the effect of calcium-induced IP_3 generation on the Ca^{2+} waves. Figure 4 shows the Ca^{2+} signals responding to the same local mechanical stimulation at $v_\delta = 0\ \mu M\,s^{-1}$. The responding Ca^{2+} signals last for no more than 140 s and the Ca^{2+} plateau only holds for 100 s. This comparison shows that the Ca^{2+}-induced IP_3 generation plays an important role to cause prolonged Ca^{2+} responding signals.

3.3. Glutamate stimulation

ICWs can also be induced by the bath applications of glutamate [1, 2]. The application of glutamate will stimulate the glutamate receptor and in turn activate PLC to generate more IP_3. Three responding types of glial cells are also classified in the experiment: sustained oscillation, damped oscillation and a step response (see figure 2 in [1]).

In the model, a stimulation term J^G_{stim} is applied to all the cells representing the glutamate bath application. At the beginning, all the cells are in steady state with $J_{stim} = 0$. At time $t = 5$ s and after that J_{stim} is turned to a high constant value J^G_{stim}. Because J^G_{stim} is applied to the cell network, all the cells show the similar oscillating Ca^{2+} signals. The trajectories of Ca^{2+} concentration at the central grid in the central cell of the network are given in figure 5.

Depending on the different values of J^G_{stim}, different Ca^{2+} waves are observed in the model. Oscillating Ca^{2+} signals can be found for J^G_{stim} in the regime of $0.0003 < J^G_{stim} < 0.005\ \mu M\,s^{-1}$ (i.e. regimes II and III in figure 2(*A*)). The oscillating periods of the intracellular Ca^{2+} signals are in the range from 45 to 12 s, as observed in experiment [1]. For $J^G_{stim} > 0.005\ \mu M\,s^{-1}$, the stable states of the cell are fixed points. But before stabilizing at the fixed point, the model cell will show a transient oscillating process. The damped oscillation response is typically found when J^G_{stim} is a little larger than $0.005\ \mu M\ s^{-1}$ (figure 5(*B*)). A higher J^G_{stim} will

induce a shorter transient oscillation, and so a large step-rise of Ca^{2+} signals is observed (figure 5(*C*)). This study points out that there is not a clear definition to distinguish the damped oscillation from the step response.

3.4. Mechanical stimulation followed by ACh bath

The application of neurotransmitter ACh can stimulate the increase of IP_3 by binding to muscarinic receptors on glial cells. Different types of Ca^{2+} responses are observed in experiment with the addition of ACh after a mechanical stimulation [11, 19]. A puzzle observed in the experiment is that for the oscillatory cells responding to mechanical stimulation, the addition of ACh can either increase the oscillatory frequency or eliminate oscillation. For the no-responding cells to mechanical stimulation, the addition of ACh can initiate oscillation [11].

In the model, all cells are set in the steady state first with $J_{stim} = 0$. Starting at time $t = 5$ s, $J^M_{stim} = 1.0\ \mu M\,s^{-1}$ is added for 15 s only to the central cell representing the mechanical stimulation. At $t = 100$ s, a term of J^A_{stim} is added to all the cells representing the application of ACh bath. Our simulation shows that different Ca^{2+} responding patterns can be observed depending on the cell position in the network and the value of J^A_{stim} applied. Two examples are given in figure 6 at $J^A_{stim} = 0.0015$ and $0.02\ \mu M\,s^{-1}$.

If the value J^A_{stim} is in the oscillation regime of $0.0003 < J^A_{stim} < 0.005\ \mu M\,s^{-1}$ (i.e. regimes II and III in figure 2(*A*)), all the cells will stabilize at a Ca^{2+} oscillating state finally. As an example, with $J^A_{stim} = 0.0015\ \mu M\ s^{-1}$ (figures 6(*A* and *B*)), although all the cells in the network will stabilize at an oscillatory state finally, but the transient Ca^{2+} signals are different, depending on the distance from the mechanically stimulated cell. As shown in figure 6(*A*), for those cells which are close to the stimulated cell, the mechanical stimulation will induce a Ca^{2+} plateau. The application of ACh will prolong this plateau (cell 2 in figure 6(*B*)). The larger the J^A_{stim}, the longer the duration of transient Ca^{2+} plateau. With mechanical stimulation, the most prominent group of cells are oscillating cells. The oscillation state can still remain with the application of Ach (cells 3 and 4 in figure 6(*B*)). But the frequency of oscillation will increase due to the increase of the IP_3 concentration (cell 4 in figure 6(*B*)). However, for the cells far from the stimulated cell, which do not show an oscillatory response to mechanical stimulation, ACh application will initiate Ca^{2+} oscillations (cell 5 in figure 6(*B*)).

If $J^A_{stim} > 0.005\ \mu M\,s^{-1}$, all the cells will stabilize at a fixed point with a high Ca^{2+} concentration finally after a transient process. An example is given in figure 6(*C*) at $J^A_{stim} = 0.02\ \mu M\,s^{-1}$. For the cells which are close to the stimulated cell, the Ca^{2+} plateau induced by the mechanical stimulation will be pushed to a higher plateau after the adding of ACh (cell 2 in figure 6(*C*)). For the oscillating cells, after ACh bath a transient oscillation is followed by a high Ca^{2+} concentration of fixed point (cells 3 and 4 in figure 6(*C*)). For those cells far from the stimulated cell, ACh induces a short duration of transient Ca^{2+} oscillation and then the cells stabilize at the fixed point (cell 5 in figure 6(*C*)).

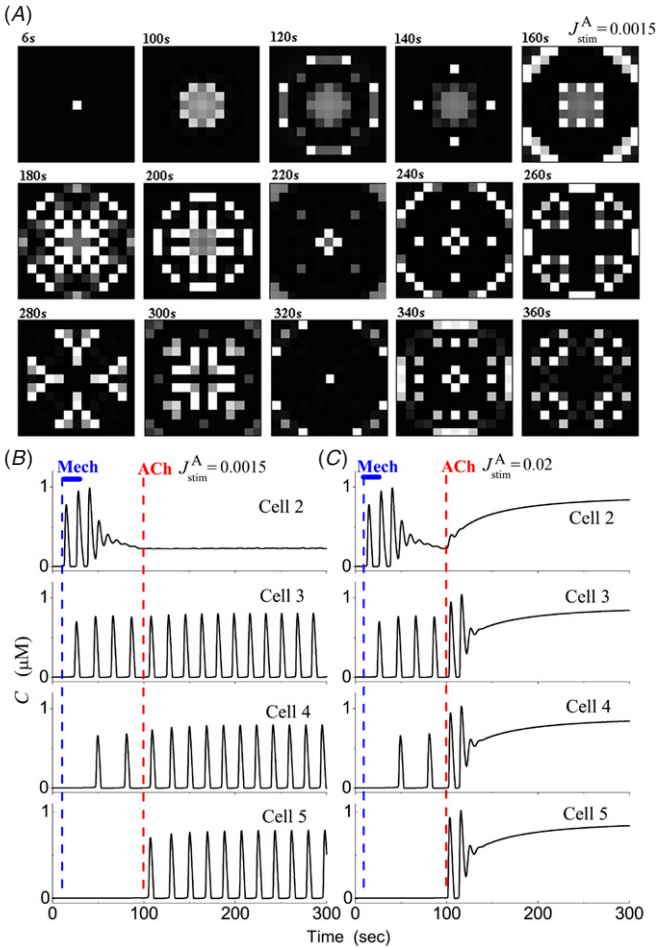

Figure 6. ICWs responding to the local mechanical stimulation followed by the application of ACh bath. Representing the local mechanical stimulation, $J^M_{stim} = 1.0\ \mu M\,s^{-1}$ is set only to the central cell for 15 s from $t = 5$ s (dashed blue line). At $t = 100$ s, a term of J^A_{stim} is added to all the cells representing the ACh bath (dashed red line). (*A*) The snapshots of intercellular Ca^{2+} waves in the cell network at $J^A_{stim} = 0.0015\ \mu M\,s^{-1}$; (*B*, *C*) The Ca^{2+} trajectory at the central grid in cells 2, 3, 4, and 5 at $J^A_{stim} = 0.0015$ and $0.02\ \mu M\,s^{-1}$, respectively.

Thus, the oscillatory cells show different responding patterns to different ACh doses. A small ACh concentration can increase the oscillation frequency (cells 3 and 4 in figure 6(*B*)), while a large ACh concentration will eliminate the cell oscillation (cells 3 and 4 in figure 6(*C*)).

3.5. Glutamate followed by mechanical stimulation

In experiment, the patterns of Ca^{2+} signals induced by glutamate followed by mechanical stimulation have also been studied [2]. It is shown that the patterns of the responding Ca^{2+} waves are similar to those observed in the absence of glutamate, but with different baselines [2].

In the model, the glutamate application means a high value of J^G_{stim} for all the cells. With a J^G_{stim}, the stable state is either a periodic oscillation with $0.0003 < J^G_{stim} < 0.005\ \mu M\,s^{-1}$ (in regime II or III in figure 2(*A*)) or a fixed point with $J^G_{stim} >$

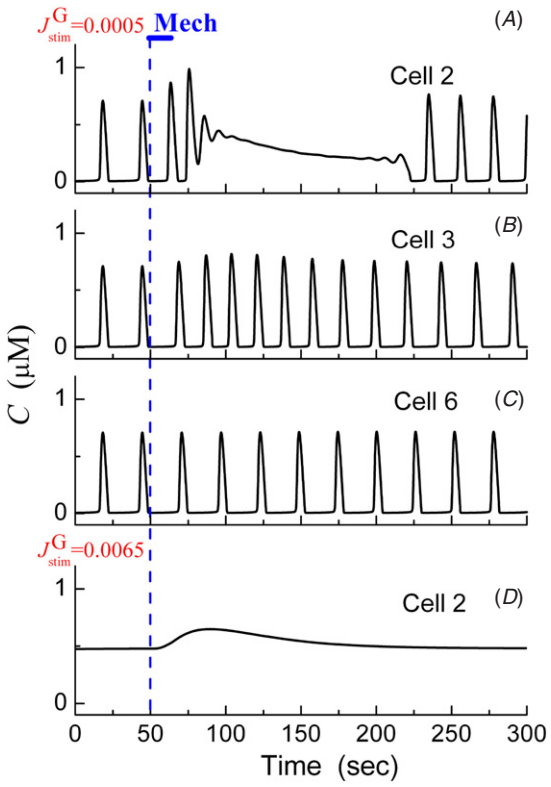

Figure 7. ICWs responding to the glutamate bath followed by local mechanical stimulation. The cell network is first in the stable states with the glutamate bath at J^G_{stim}. Then $J^M_{stim} = 1.0\ \mu M\,s^{-1}$ is set only to the central cell for 15 s representing the local mechanical stimulation (dashed blue line). (*A*–*C*) The Ca^{2+} signals with glutamate bath at $J^G_{stim} = 0.0005\ \mu M\,s^{-1}$ for cells 2, 3, and 6, respectively; (*D*) the Ca^{2+} wave of cell 2 with glutamate bath at $J^G_{stim} = 0.0065\ \mu M\,s^{-1}$.

$0.005\ \mu M\,s^{-1}$ (in regime IV in figure 2(*A*)). The latterly added local mechanical stimulation at the central cell will generate a higher IP_3 concentration, spreading to the nearby cells around the stimulated cell. However, the IP_3 degradation will drive the high IP_3 concentration back to its stable state corresponding to J^G_{stim}. So the mechanical stimulation will induce a transient and localized waves overlapping on the steady oscillating state or fixed point state.

Figures 7(*A*)–(*C*) show the simulation results with $J^G_{stim} = 0.0005\ \mu M\,s^{-1}$, where the stable state of each cell is a periodic oscillation. From time $t = 50$ s, the central cell is mechanically stimulated with $J^M_{stim} = 1.0\ \mu M\,s^{-1}$ for 15 s. For the cells close to the stimulated cell, a high IP_3 concentration is generated, resulting in a Ca^{2+} plateau after a transient process of oscillation (figure 7(*A*)). For the cells which are not so far away from the stimulated cell, the oscillating frequency becomes faster soon after the mechanical stimulation, due to a higher IP_3 concentration (figure 7(*B*)). For the far-distanced cells, the mechanical stimulation has little effect (figure 7(*C*)).

Another example is shown in figure 7(*D*) at $J^G_{stim} = 0.0065\ \mu M\,s^{-1}$. For this example, no oscillation will be found in the cells, and the mechanical stimulation only causes a transient of high Ca^{2+} peak, which is also observed in experiment [2].

4. Discussion and conclusion

In this paper, a model has been proposed for intercellular Ca^{2+} waves and compared with the experimental data observed in glial cells. In the model, we consider a small term of Ca^{2+}-induced IP_3 regeneration and assume that IP_3 is the major component carrying the signal through gap junctions between glial cells. The intracellular Ca^{2+} model has a bistable dynamics in a large regime of IP_3 concentration, which is quite different from the other Ca^{2+} models [14–24, 28, 29], in which the oscillating state is typically found alone.

With the model we systematically discuss experimental observations in glial cells responding to different stimulations, i.e. local mechanical stimulation [11], glutamate application [1], mechanical stimulation followed by ACh application [11], and glutamate followed by mechanical stimulation [2]. In the model, the local mechanical stimulation causes a high IP_3 concentration in the stimulated cell, which then diffuses to the nearby cells with a degradation dynamics. The bath of ACh or glutamate causes a high IP_3 generation rate for all the cells. Different Ca^{2+} patterns observed in the experiments are explained by the transitions of the cells among different dynamical states: fixed point, oscillating state or bistable state.

It has been suggested that the Ca^{2+}-induced IP_3 regeneration is not a necessary term [18–20] for ICWs. However, Hofer *et al* showed that a model with such a term can account for many features observed in experimental ICWs [23]. Later, Ullah *et al* suggested that it is a necessary factor to achieve the anti-phase synchronization observed in experiment [25]. We show in this paper that only after including a small term of Ca^{2+}-induced IP_3 generation, the model can give a quite prolonged Ca^{2+} wave, as well as a prolonged Ca^{2+} plateau, responding to mechanical stimulation, as observed in experiment [11]. The term of Ca^{2+}-induced IP_3 regeneration directly causes more IP_3 messengers to be generated so as to induce a longer duration of Ca^{2+} wave.

With the bistable Ca^{2+} model, we can easily reproduce the prolonged Ca^{2+} plateau for the cells that are close to the mechanically stimulated cell. This is because, when the decreased IP_3 concentration falls from the fixed point regime to the bistable regime, the cell will still keep the fixed point dynamics, resulting in a prolonged plateau. Such a large regime of bistable dynamics makes our intracellular Ca^{2+} model quite different from the other Ca^{2+} models. It is not clear, however, if such a bistable behavior can be observed or confirmed in the experiment.

There is a paradoxical observation in the experiment with mechanical stimulation followed by ACh application. In detail, for the oscillating cells responding to mechanical stimulation, the addition of ACh can either increase the oscillating frequency or eliminate oscillation [11]. With the model, we show that the effects of ACh bath on the oscillating cells are depending on the ACh concentration applied. A small ACh concentration will not change the oscillation state of cells, but the oscillation frequency will increase due to the increase of IP_3 concentration. In contrast, a large ACh concentration will drive the cell to a fixed point state at high IP_3 concentration, eliminating the cell oscillation.

In the model the IP_3 responses to glutamate and ACh bath are both simply modeled by the generation rate J_{stim}. This is because we only concern that a certain IP_3 concentration will be generated in the cell and so we ignore the detailed dose-responding dynamics between IP_3 generation and glutamate or ACh bath. However, experiment also showed that astrocytes can release glutamate in a Ca^{2+}-dependent manner within an appropriate range of astrocytic calcium levels and consequently may signal to adjacent cells, giving a complex dynamics for glutamate bath [37]. Another experiment indicated that neuronal nicotinic acetylcholine receptors (nAChRs) are present on hippocampal astrocytes and their activation responding to ACh bath can directly produce a calcium current, giving another pathway to modulate the Ca^{2+} signal [38]. We suggest that a detailed model including these effects remains a further investigation.

Similar to many ICW models [14–16, 18–22], we consider here a deterministic signal dynamics with homogeneous and symmetry cell structure. Thus, the simulated ICWs are symmetric and regular. The biologically realistic features, such as clustering distribution of IP_3Rs, the stochastic channel dynamics, and the heterogeneities of gap junctional permeability and cell Ca^{2+} dynamics, have not been considered. One can expect that these factors can affect the intracellular and also intercellular Ca^{2+} waves, as discussed, for example, in [23, 26]. The appearance of the ICWs with a model considering these factors will be considerably closer to the experimental observations and provide more quantitative insights in ICWs.

Acknowledgments

We acknowledge support by Ministry of Education of China under grant 108075 and National Science Foundation of China under grants 10775114 and 30970970.

References

[1] Cornell-Bell A H, Finkbeiner S M, Cooper M S and Smith S J 1990 Glutamate induces calcium waves in cultured astrocytes: long-range glial signaling *Science* **247** 470–3
[2] Charles A C, Merrill J E, Dirksen E R and Sanderson M J 1991 Intercellular signaling in glial cells: calcium waves and oscillations in response to mechanical stimulation and glutamate *Neuron* **6** 983–92
[3] Charles A 1998 Intercellular calcium waves in glia *Glia* **24** 39–49
[4] Venance L, Piomelli D, Glowinski J and Giaume C 1995 Inhibition by anandamide of gap junctions and intercellular calcium signalling in striatal astrocytes *Nature* **376** 590–5
[5] Giaume C and Venance L 1998 Intercellular calcium signaling and gap junctional communication in astrocytes *Glia* **24** 50–64
[6] Fields R D and Stevens-Graham B 2002 Neuroscience—new insights into neuron-glia communication *Science* **298** 556–62
[7] Allen N J and Barres B A 2009 Glia—more than just brain glue *Nature* **457** 675–7
[8] Fiacco T A, Agulhon C, Taves S R, Petravicz J, Casper K B, Dong X, Chen J and McCarthy K D 2007 Selective stimulation of astrocyte calcium *in situ* does not affect neuronal excitatory synaptic activity *Neuron* **54** 611–26
[9] Newman E A 2001 Propagation of intercellular calcium waves in retinal astrocytes and muller cells *J. Neurosci.* **21** 2215–23
[10] Newman E A and Zahs K R 1997 Calcium waves in retinal glial cells *Science* **275** 844–7
[11] Strahonja-Packard A and Sanderson M J 1999 Intercellular Ca^{2+} waves induce temporally and spatially distinct intracellular Ca^{2+} oscillations in glia *Glia* **28** 97–113
[12] Arcuino G, Lin J H C, Takano T, Liu C, Jiang L, Gao Q, Kang J and Nedergaard M 2002 Intercellular calcium signaling mediated by point-source burst release of ATP *Proc. Natl Acad. Sci. USA* **99** 9840–5
[13] Scemes E, Suadicani S O and Spray D C 2000 Intercellular communication in spinal cord astrocytes: fine tuning between gap junctions and P2 nucleotide receptors in calcium wave propagation *J. Neurosci.* **20** 1435–45
[14] Goldberg M, De Pitta M, Volman V, Berry H and Ben-Jacob E 2010 Nonlinear gap junctions enable long-distance propagation of pulsating calcium waves in astrocyte networks *PLOS Comput. Biol.* **6** e1000909
[15] Wilkins M and Sneyd J 1998 Intercellular spiral waves of calcium *J. Theor. Biol.* **191** 299–308
[16] Dupont G, Tordjmann T, Clair C, Swillens S, Claret M and Combettes L 2000 Mechanism of receptor-oriented intercellular calcium wave propagation in hepatocytes *FASEB J.* **14** 279–89
[17] Gracheva M E, Toral R and Gunton J D 2001 Stochastic effects in intercellular calcium spiking in hepatocytes *J. Theor. Biol.* **212** 111–25
[18] Sneyd J, Charles A C and Sanderson M J 1994 A model for the propagation of intercellular calcium waves *Am. J. Physiol. Cell Physiol.* **266** C293–302
[19] Sneyd J, Wilkins M, Strahonja A and Sanderson M J 1998 Calcium waves and oscillations driven by an intercellular gradient of inositol (1,4,5)-trisphosphate *Biophys. Chem.* **72** 101–9
[20] Sneyd J, Wetton B T, Charles A C and Sanderson M J 1995 Intercellular calcium waves mediated by diffusion of inositol trisphosphate: a two-dimensional model *Am. J. Physiol.* **268** C1537–45
[21] Nakano T, Shuai J, Koujin T, Suda T, Hiraoka Y and Haraguchi T 2010 Biological excitable media based on non-excitable cells and calcium signaling *Nano Commun. Netw.* **1** 43–9
[22] Hofer T, Politi A and Heinrich R 2001 Intercellular Ca^{2+} wave propagation through gap-junctional Ca^{2+} diffusion: a theoretical study *Biophys. J.* **80** 75–87
[23] Hofer T, Venance L and Giaume C 2002 Control and plasticity of intercellular calcium waves in astrocytes: a modeling approach *J. Neurosci.* **22** 4850–9
[24] Iacobas D A, Suadicani S O, Spray D C and Scemes E 2006 A stochastic two-dimensional model of intercellular Ca^{2+} wave spread in glia *Biophys. J.* **90** 24–41
[25] Ullah G, Jung P and Cornell-Bell A H 2006 Anti-phase calcium oscillations in astrocytes via inositol (1, 4, 5)-trisphosphate regeneration *Cell Calcium* **39** 197–208
[26] Shuai J W and Jung P 2003 Optimal ion channel clustering for intracellular calcium signaling *Proc. Natl Acad. Sci. USA* **100** 506–10
[27] Smith I F, Wiltgen S M, Shuai J and Parker I 2009 Ca^{2+} puffs originate from preestablished stable clusters of inositol trisphosphate receptors *Sci. Signal.* **2** ra77
[28] DeYoung G W and Keizer J 1992 A single-pool inositol 1,4,5-trisphosphate-receptor-based model for agonist-stimulated oscillations in Ca^{2+} concentration *Proc. Natl Acad. Sci. USA* **89** 9895–9
[29] Li Y X and Rinzel J 1994 Equations for InsP3 receptor-mediated Ca^{2+} oscillations derived from a detailed

kinetic-model: a Hodgkin–Huxley like formalism *J. Theor. Biol.* **166** 461–73
[30] Swillens S, Dupont G, Combettes L and Champeil P 1999 From calcium blips to calcium puffs: theoretical analysis of the requirements for interchannel communication *Proc. Natl Acad. Sci. USA* **96** 13750–5
[31] Sneyd J and Dufour J F 2002 A dynamic model of the type-2 inositol trisphosphate receptor *Proc. Natl Acad. Sci. USA* **99** 2398–403
[32] Shuai J, Pearson J E, Foskett J K, Mak D D and Parker I 2007 A kinetic model of single and clustered IP_3 receptors in the absence of Ca^{2+} feedback *Biophys. J.* **93** 1151–62
[33] Kang M and Othmer H G 2007 The variety of cytosolic calcium responses and possible roles of PLC and PKC *Phys. Biol.* **4** 325–43
[34] Nadkarni S and Jung P 2007 Modeling synaptic transmission of the tripartite synapse *Phys. Biol.* **4** 1–9
[35] Allbritton N L, Meyer T and Stryer L 1992 Range of messenger action of calcium-ion and inositol 1,4,5-trisphosphate *Science* **158** 1812–5
[36] Wang S S H, Alousi A A and Thompson S H 1995 The lifetime of inositol 1,4,5-trisphosphate in single cells *J. Gen. Physiol.* **105** 149–71
[37] Parpura V and Haydon P G 2000 Physiological astrocytic calcium levels stimulate glutamate release to modulate adjacent neurons *Proc. Natl Acad. Sci. USA* **97** 8629–34
[38] Sharma G and Vijayaraghavan S 2001 Nicotinic cholinergic signaling in hippocampal astrocytes involves calcium-induced calcium release from intracellular stores *Proc. Natl Acad. Sci. USA* **98** 4148–53